

RESEARCH ARTICLE

Study on Wind Vibration Response and Coupling Effect of Transmission Tower-Line System Under Downburst

YONGLI ZHONG¹, YICHEN LIU¹, SHUN LI², ZHITAO YAN^{1,3}, AND XINPENG LIU¹¹School of Civil Engineering and Architecture, Chongqing University of Science and Technology, Chongqing 401331, China²Chongqing IAT Automobile Research Institute Company Ltd., Chongqing 401121, China³School of Civil Engineering, Chongqing University, Chongqing 400045, China

Corresponding author: Zhitao Yan (zhitaoan@qq.com)


This work was supported in part by the National Natural Science Foundation of China under Grant 52178458 and Grant 52008070, in part by the Natural Science Foundation of Chongqing, China under Grant CSTB2024NSCQ-MSX1135, in part by the Project funded by China Postdoctoral Science Foundation under Grant 2023M734084, in part by the Natural Science Foundation of Chongqing Municipality under Grant CSTB2023NSCQ-LZX0051, and in part by Chongqing Bayu Scholars Program under Grant YS2023091.

ABSTRACT Downburst is a type of near-surface short-term destructive strong wind that significantly affects wind-sensitive flexible structures like transmission tower-line systems. The existence of the tower-line coupling effect complicates the wind-induced vibration response analysis. Firstly, the average wind speed time history is obtained using the impinging jet wind field model, the pulsating wind speed time history is simulated using the harmonic synthesis method, and then the total wind speed time history of the downburst is obtained by superposition. Then, the transmission tower-line finite element model is established to carry out the wind vibration response analysis under different wind attack angles. Based on the most unfavorable wind angle of attack, the wind-induced vibration response and the coupling effect of the tower-line system are investigated under different maximum wind speed heights (Z_{\max}) and span distances. Finally, the range of wind load reduction coefficients for the tower-line separation system is given. The results show that under the most unfavorable wind angle of attack, both the displacement and acceleration response of the tower-line separation system are more significant than that of the tower-line coupling system. At $Z_{\max} = 70$ m, the difference in displacement response between the two systems reaches the maximum, indicating an apparent tower-line coupling effect. As the span distance increases, both the displacement response and the acceleration response of the tower-line separation system increase. In contrast, the displacement response of the tower-line coupling system increases, but the acceleration response decreases. For the proposed design reduction coefficient for the transmission tower-line coupling effect under the action of the downburst, it is considered more reasonable to take the value between 0.83-0.95. This study provides some references for further optimization of the transmission tower design.

INDEX TERMS Downburst, computational fluid dynamics (CFD), transmission tower-line system, wind-induced vibration response, tower-line coupling effect.

I. INTRODUCTION

The transmission tower-line system is an integral part of the power transmission system. They have a large span, high flexibility, strong geometric nonlinearity, etc. Once it

The associate editor coordinating the review of this manuscript and approving it for publication was Tariq Masood .

is affected by high-intensity winds during operation, it seriously threatens the safety and stability of the entire circuit system. Downburst is a localized strong convective weather phenomenon, a strong near-surface wind with significant impact caused by the downdraft impacting the ground and diffusing around. During thunderstorms, the probability of occurrence of microbursts can reach 60%-70% [1], the

maximum wind speed can reach 75 m/s [2], and the maximum wind height usually occurs at 25-100 m from the ground [3]. Investigations have shown that over 80% of weather-related transmission line failures worldwide are caused by downburst events [4]. Still, the current research on the wind vibration response of transmission tower-line systems under the action of downbursts has not yet met the design requirements.

Considering that the structure of the downburst wind field is close to that of the impinging jet, most researchers have used the impinging jet model to investigate the wind field characteristics of the downburst. Earlier, Selvam and Holmes [2] used a two-dimensional (2D) impinging jet model for numerical simulation to investigate the effect of downburst on the design wind speed of the structure. Wood et al. [5] used an impinging jet device to study the wind field of downbursts in different terrains. Based on the experimental results, they proposed an empirical expression for the horizontal wind speed and vertical wind profile. Letchford and Chay [6] simulated the wind field characteristics of a moving downburst using a nozzle-facing upward-impinging jet device, and the pressure distribution on the surface of a cube was investigated. Sengupta et al. [7] combined numerical simulations and physical experiments to study the effects of a downburst on a building. Abd-Elaal et al. [8] developed a three-dimensional (3D) impinging jet model of a 1/8 cylinder to investigate the distribution of downburst wind speed over the actual terrain. Fang et al. [9] investigated the wind field characteristics of stationary and moving downbursts by a mobile impinging jet device mounted on a steel frame.

In recent years, numerous studies have been conducted on the response characteristics of transmission tower-line systems under downbursts. Shehata et al. [10] conducted CFD simulations of downburst wind speed time history, analyzed the response of transmission tower-line systems under downburst, and found that the peak axial force of the transmission tower members under downburst exceeded the peak axial force of the members under the wind in the atmospheric boundary layer by about 9%-304%, which suggests that the critical loads of downburst wind should be fully considered when designing transmission lines. Fu et al. [11] investigated the response characteristics of transmission towers under the combined effect of wind and rain loads. They found that rain loads significantly impact transmission tower damage and should be focused on during weather like thunderstorms and high winds. Damatty and Elawady [12] conducted an extensive parametric study of different transmission lines to evaluate their critical response to downburst loads. Zhao et al. [13] investigated the frequency and time domain response characteristics of the wind vibration response of transmission towers under different moving downburst conditions. Liu et al. [14] studied the wind vibration response characteristics of transmission towers under different wind direction angles using a thunderstorm-impinging wind simulator. Yu and Li [15] established a method suitable for nonlinear response analysis of large structures and can

simulate complex nonlinear behavior. Fu et al. [16] studied the response characteristics of transmission towers under various extreme loading conditions through full-scale tests and numerical simulations. Alawode et al. [17] compared the wind vibration response of transmission towers under downburst and atmospheric boundary layer winds through wind tunnel tests and found that transmission towers may be subjected to more wind-induced vibrations under downburst winds with peak wind speeds like those of atmospheric boundary layer winds.

In China, wind load is usually calculated using a single tower calculation for the transmission tower design. However, the transmission tower in the line after the coupling effect is not considered. Guo [18] found that the resonance response of a tower-line system was lower than that of a single tower, and the background response was higher through finite element analysis and the wind tunnel test of the air-elastic model. Meanwhile, it is pointed out that the impact of the tower-line coupling effect on wind vibration response should be fully considered in the design of transmission towers. He et al. [19] analyzed the stability of the tower-line system under wind load and showed that the impact of the tower-line coupling effect should be considered in the design of the transmission tower. Li [20] established the transmission tower-line coupling finite element model and analyzed the tower and conductor displacement and force in different wind direction angles under the rule of change. Zhang et al. [21] established an uncoupled tower-line model for wind vibration response analysis. They found that the results match better when compared with the tower-line coupled model, which reduces the computational cost. Wu et al. [22] performed numerical simulations of tower-line separation and coupling systems. They found that the tower-line coupling effect causes frequent fluctuations in the stress and displacement response of the tower. Zhu et al. [23] investigated the random wind field characteristics and wind-induced vibration response under the tower-line coupled system, which showed that aerodynamic damping can significantly reduce the downwind amplitude of the conductors and shield wires. Zhang [24] studied the effect of different slopes and wind direction angles on the coupling effect of transmission towers and lines and found that the wind vibration response of transmission towers in the uncoupled system is more significant than that of the coupled system. Fang et al. [25] studied the wind vibration response of a single tower and tower-line system under a downburst. Meanwhile, they considered the effect of the wind field parameters related to the mean wind profile on the wind vibration response of the tower-line system. As seen from the above, previous studies have shown that the traditional transmission tower design is unreasonable, and the coupling effect of tower-line interaction needs to be considered; most of the earlier studies are based on the atmospheric boundary layer wind field. The wind vibration response of the transmission tower-line system under the action of downburst and the tower-line coupling effect is

less studied and less involved in its closely related impact parameters.

Based on the existing research, this paper analyzes the wind vibration response and tower-line coupling effect of the transmission tower-line system under the action of downburst using ANSYS. Section II describes the simulation of the total wind speed time history of the downburst. Section III presents the finite element modeling of the transmission single tower and tower-line system. Section IV-A determines the most unfavorable wind angle of attack for the tower-line system under downburst. Section IV-B analyzes the displacement and acceleration response of the two tower-line systems under downburst. Sections IV-C and IV-D analyze the displacement and acceleration responses of the two tower-line systems under different maximum wind heights (Z_{max}) and span distances. Section IV-E presents the design reduction coefficient for the coupling effect of the tower-line system under the downburst and gives the reference range of values.

II. DOWNBURST WIND LOAD

A. DOWNBURST MEAN WIND SPEED SIMULATION

In the downburst wind field simulation, Hangan et al. [26] found two sets of initial conditions with excellent agreement with the measured data by investigating the downburst wind speed time history. The initial velocity is $V_{jet} = 29$ m/s, $D = 600$ m, when $H/D = 4$, and $D = 950$ m when $H/D = 2$. The computational model parameters in this paper are formulated as $V_{jet} = 29$ m/s and $D = 600$ m. The geometrical scaling is 1:2000, the speed scaling is 1:3, and the time scaling is 1:1000, which aligns with that recommended by Mason et al. [27]. According to the analysis of measured data, the actual downburst wind field is spatially symmetric. To save computational resources, a 2D axisymmetric impinging jet model is used for the calculation, and the computational domain is set to be $10D_{jet} \times 10D_{jet}$. The velocity inlet is $4D_{jet}$ away from the ground, ensuring the jet can fully develop. The computational domain of the downburst wind field used in this paper is shown in Figure 1, and the corresponding boundary conditions are set as shown in Table 1.

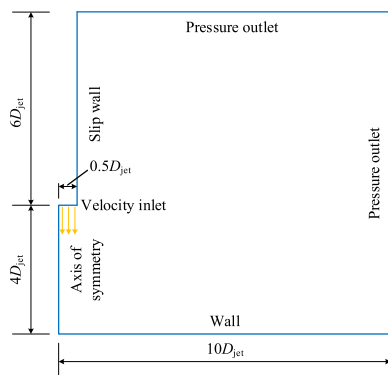


FIGURE 1. Schematic of the computational domain.

In this paper, ANSYS finite element software FLUENT 19.0 is utilized for the numerical simulation of the impinging jet. The Reynolds-averaged Navier-Stokes (RANS) method and the Reynolds Stress Model (RSM) turbulence model are chosen for the solution. A discrete solver is used for solving the governing equations, the coupled pressure and velocity fields are solved using the SIMPLEC algorithm, the spatial discretization of the fluid is in the second-order upwind format, and momentum, turbulence kinetic energy, turbulence energy dissipation rate, and Reynolds stress are discretized using the QUICK format [28].

TABLE 1. Boundary condition setting.

Boundary type	Boundary condition
Velocity inlet	$V_{jet} = 7.5$ m/s, $I_u = 1\%$, $R = D_{jet}$
Axis of symmetry	AXIS
Wall	Enhanced wall treatment
Pressure outlet	$I_u = 1\%$, $R = D_{jet}$
Slip wall	Zero shear stress

The ICEM CFD module is used for the structured meshing of the 2D model. They are considering the significant impact on the wall boundary when the fluid exits the flow and the complexity of the flow inside the fluid; thus, the inlet and bottom meshes of the computational domain are encrypted. Typically, the distance from the first grid of the wall is defined as the dimensionless distance y^+ , and limited to less than 1 to ensure the rationality of the grid layout. Where $y^+ = \Delta y \rho u_\tau / \mu$, u_τ is the wall friction velocity, $u_\tau = (\tau_w / \rho)^{1/2}$, Δy is the distance from the first layer of the grid to the wall, τ_w is the wall shear stress, μ is the dynamic viscosity of the fluid, and ρ is the air density. By verifying Δy , the total number of grids in the computational domain of the impinging jet model is about 120,000.

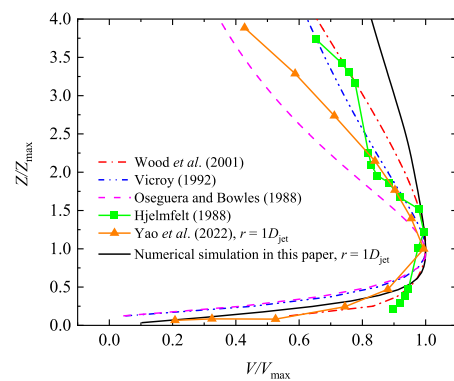


FIGURE 2. Comparison of mean wind profiles.

The vertical wind profile at $r = 1D_{jet}$ obtained from the simulation in this paper is compared with the three classical empirical models of downburst proposed by Vicroy [29], Oseguera and Bowles [30], and Wood et al. [5], the Hjelmfelt [3] averaged measured data, and Yao [31] wind tunnel test results, as shown in Figure 2. Figure 2 shows that in the

part below $Z/Z_{\max} = 1$ height, the CFD simulation results are close to the above literature results. However, in the part above $Z/Z_{\max} = 1$ height, the CFD simulation results are more significant than the results of other studies. This is because the duration of the downburst is short, and the downdraft flow is not stable, while the CFD simulation results result from the flow field reaching a stationary state. In addition, the effect of the roughness of the actual surface on the flow field is not considered in the simulation in this paper.

The downburst wind speeds at $r=1D_{\text{jet}}$ obtained from CFD simulations are given in Figure 3, and five different heights with Z/D_{jet} of 0.005, 0.01, 0.015, 0.0175, and 0.02 are taken. From Figure 3, we can see that at various heights, the downburst wind speeds as a whole show a rapid rise to form the first peak, then the wind speeds rapidly decline, then rise to create the second peak, and then gradually stabilize, which is in line with the characteristics of the downburst wind field.

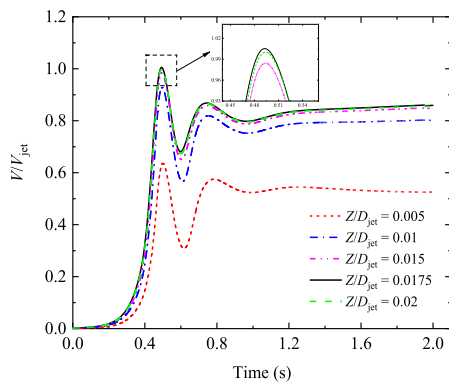


FIGURE 3. Mean wind speed time history of downburst.

B. DOWNBURST PULSATING WIND SPEED SIMULATION

The downburst wind speed can be viewed as a superposition of pulsating and average winds, and the downburst wind speed is expressed as:

$$U(z, t) = \bar{U}(z, t) + u(z, t) \quad (1)$$

where $\bar{U}(z, t)$ is the average wind speed and $u(z, t)$ is the pulsating wind speed.

The downburst pulsating wind and mean wind are both a non-stationary stochastic process. Chen and Letchford [32] considered the maximum value of pulsating wind speed to be about 25% of the mean wind speed at that time, while Chay [33] considered it 8%-11%. Therefore, it can be expressed as [32]:

$$u(z, t) = \alpha(z, t)k(z, t) \quad (2)$$

where the time-varying amplitude modulation function is $\alpha(z, t) = 0.08\bar{U}(z, t) \sim 0.11\bar{U}(z, t)$ taken, and $\alpha(z, t) = 0.1\bar{U}(z, t)$ is taken in this paper, $k(z, t)$ is a Gaussian smooth stochastic process obeying a standard normal distribution.

The downburst pulsating wind speed is transformed into a uniform, unsteady stochastic process, and the self-spectral

density function can be expressed as:

$$S_{zz}(z, t, \omega) = |\alpha(z, t)|^2 \times \varphi(z, \omega) \quad (3)$$

where $S_{zz}(z, t, \omega)$ is the auto spectral density, $\varphi(z, \omega)$ is the power spectral density (PSD), and ω is the frequency parameter.

The downburst pulsating wind speeds at two points in space are correlated, and taking the correlation coefficient at the two points as $\gamma(z_1, z_2, \omega)$, the PSD of the wind speed time history acting at each end of the structure can be written as:

$$S(t, \omega) = A(t)\Phi(\omega)\bar{A}^T(t) \quad (4)$$

where $A(t) = [\alpha(z_1, t), \alpha(z_2, t), \dots, \alpha(z_n, t)]$, $\bar{A}^T(t)$ is the $A(t)$ conjugate transpose matrix, $\Phi(\omega)$ is the PSD matrix of the vector $k(t) = [k(z_1, t), k(z_2, t), \dots, k(z_n, t)]^T$.

Jiang et al. [34] proposed a new matrix factorization-assisted interpolation method, which can significantly reduce the number of Cholesky decompositions and acceleration of harmonic superposition with a small number of fast Fourier transforms (FFTs). The wind field simulation program uses MATLAB software according to the above method. Since the transmission tower-line system is a towering structure, the Kaimal spectrum, which reflects the effect of height on the wind spectrum, is used as the target spectrum. The harmonic synthesis method is utilized to generate the pulsating wind speed time history from the CFD mean wind speed time history, and the pulsating wind speed time history of the downburst at a height of 25 m is shown in Figure 4, from which we can see that the pulsating wind amplitude is positively correlated with the mean wind.

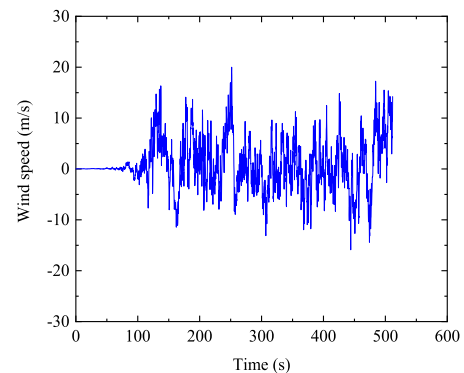


FIGURE 4. Time history of downburst pulsating wind speed at 25 m height.

C. DOWNBURST WIND SPEED SIMULATIONS AT DIFFERENT HEIGHTS

The average wind speed time history is scaled on the previous CFD simulation results following the scaling technique proposed by Shehata et al. [10]. By using three interpolation functions to scale and interpolate the wind speed at any given transmission tower node, conductor, and ground wire, the

wind speed time history at each node height of the transmission tower is simulated with the following expression:

$$\begin{cases} Z_f = Z_m \times \frac{D_{Jf}}{D_{Jm}} \\ r_f = r_m \times \frac{D_{Jm}}{D_{Jf}} \\ V_f = V_m \times \frac{V_{Jf}}{V_{Jm}} \end{cases} \quad (5)$$

where r_f and Z_f are radial and vertical coordinates, respectively, D_{Jf} and V_{Jf} are full-scale parameters of the downburst, with D_{Jf} taking values between 500 m and 1500 m, and the velocity $V_{Jf} = 70$ m/s, representing typical extreme wind speeds recorded during downburst events [35].

The downburst wind speed time scale at any height can be obtained by superimposing the average wind speed and pulsating wind speed in the above method. For the space limitation, this paper only gives the downburst wind speed time history and power spectrum at the height of 75 m of the transmission tower, as shown in Figure 5. From Figure 5(a), we can see that the pulsating wind speed of the downburst is related to the average wind speed, which peaks at 100-200 s, and the pulsating wind speed increases. Meanwhile, the downburst wind speed increases gradually with the increase in height, and the peak wind speed of the downburst exceeds 80 m/s at 75 m. From Figure 5(b), we can see that the simulated pulsating wind PSD matches the target spectra (Kaimal spectra) exceptionally well, which ensures the accuracy of the wind speed time history simulation.

III. FINITE ELEMENT MODEL OF TRANSMISSION TOWER-LINE SYSTEM

A. FINITE ELEMENT MODEL AND DYNAMIC CHARACTERISTICS OF TRANSMISSION TOWER

This paper uses a 500 kV DC large-span transmission tower as a finite element model. Modeled by ANSYS finite element software, the transmission tower is divided into ten sections in the height direction, referred to as panels, and the finite element model is shown in Figure 6.

TABLE 2. Natural frequency and mode description of tower model.

Order	Natural frequency (n/HZ)	Mode shapes
1	1.6245	First-order bending mode in the line direction
2	1.6449	First-order bending mode of vertical line direction
3	3.9059	First-order torsional mode

Considering that the transmission tower has strong geometric nonlinearity, spatial beam element BEAM188 is used to simulate the angle steel rods of the transmission tower. The primary material of the transmission tower and the cross-arm are made of Q345 steel with high strength, good toughness, and good welding performance, and the diagonal material of the transmission tower and other auxiliary materials are made of Q235 steel with high plasticity and low cost, which

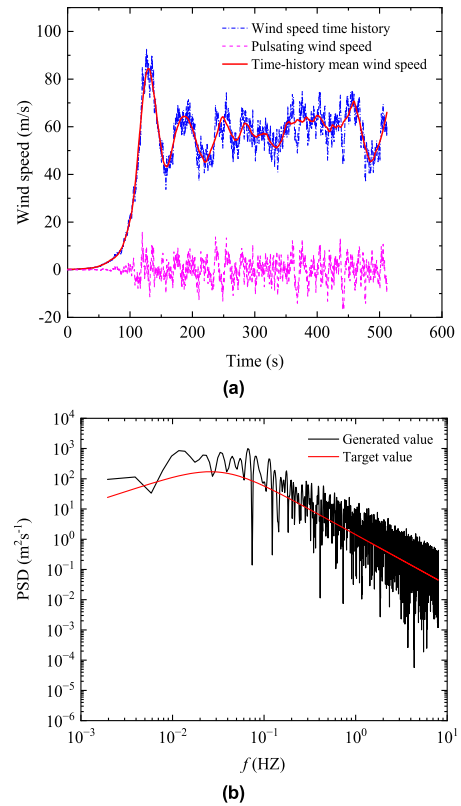


FIGURE 5. Comparison of time history and power spectrum of downburst wind speed at 75 m height.

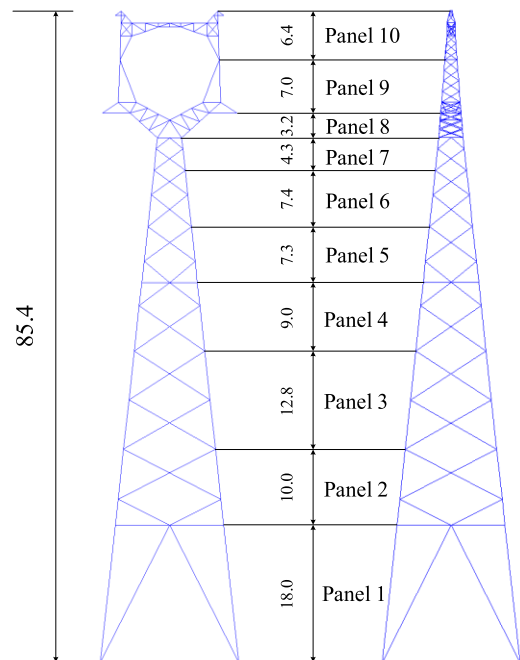


FIGURE 6. Finite element model of transmission tower (Unit: m).

can meet the various performance requirements of the transmission tower. Constrain all the degrees of freedom of the

four nodes at the bottom of the transmission tower. The modal analysis function of ANSYS is used to calculate the modal of the transmission tower structure using the block Lanczos method, which is computationally efficient and particularly suitable for analyzing large structures. Table 2 lists the first three orders of vibration frequencies and vibration descriptions of the transmission tower, and the corresponding vibration modes of the transmission tower are given in Figure 7.

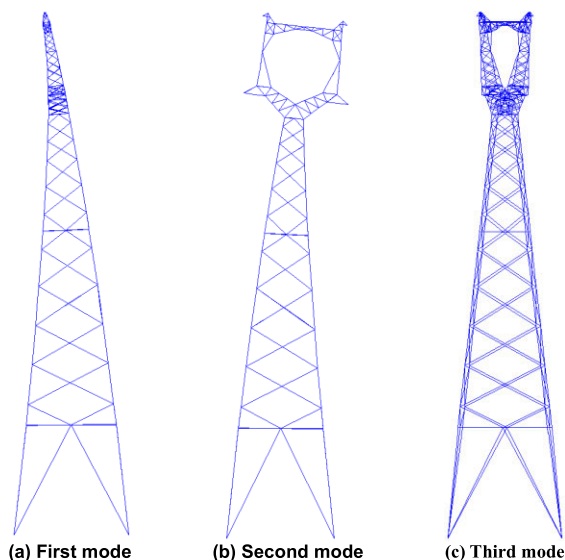


FIGURE 7. The first three modes of transmission tower.

B. FINITE ELEMENT MODEL OF TRANSMISSION TOWER-LINE SYSTEM AND DYNAMIC CHARACTERISTICS

Zhu [36] analyzed the wind vibration response of the finite element model of transmission tower line with different span numbers and found that the mean and maximum values of displacement and axial force are equal under various spans. Therefore, the “one tower and two lines” finite element model is used for calculation to improve the computational efficiency. By adding insulator strings, conductors, and ground wires models to the transmission tower, all the degrees of freedom of the four nodes at the bottom of the tower, conductor, and ground endpoints are constrained, thus obtaining the finite element model of the transmission tower-line system, as shown in Figure 8.

The conductors and ground wire are 550 m long, assumed to be mainly subjected to tensile force without bending moment and pressure, and have strong nonlinearity. To reduce the amount of calculation in the modeling, according to the principle of equivalence of physical parameters such as cross-sectional area, the complex multiple conductors are converted into a single conductor model, which is simulated by the LINK10 element. The transmission line is divided into three layers; the first layer is two ground wires, a diameter of 16 mm, a modulus of elasticity 1.85×10^{11} N/mm², Poisson’s

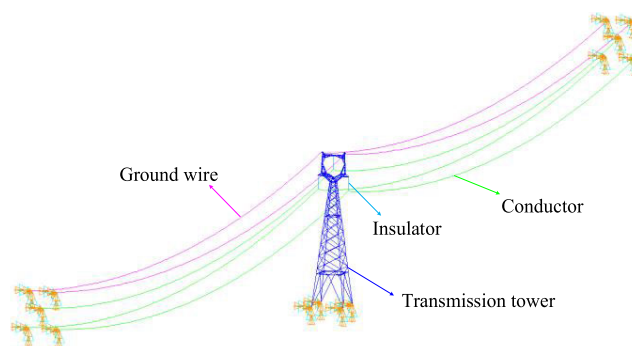


FIGURE 8. Finite element model of the tower-line system.

ratio of 0.3, and a unit length of the mass of 1.2 kg/m. The second and the third layers are, respectively, one group of conductors and two groups of conductors, with a diameter of 32 mm, the elasticity of the modulus of elasticity is 6.3×10^{10} N/mm², Poisson’s ratio is 0.3, the unit length of the mass of 1.9 kg/m. The analytical method is used for shape-finding analysis of conductors and grounds, with methodological reference [37], which will not be described here.

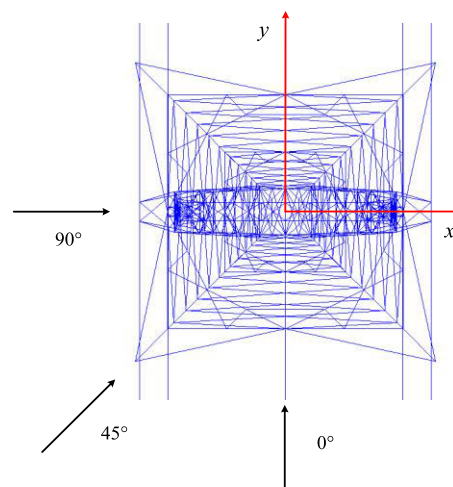


FIGURE 9. Diagram of wind angle of attack of transmission tower.

In engineering practice, the transmission tower-line system will be subjected to wind loads from all directions. The wind load angle perpendicular to the transmission conductor is defined as 90°, and the angle parallel to the transmission conductor is defined as 0°. The wind angle of the attack schematic is shown in Figure 9.

The modal analysis of the tower-line system is carried out using the block Lanczos method. The first 71st-order vibration modes of the tower-line system are all conductor and ground wire vibration modes. The vibration modes induced by the transmission tower appear as early as in the 72nd-order vibration mode, and the first three-order vibration modes induced by the transmission tower are shown in Figure 10. Figure 10 shows that the first-order primary vibration mode

is bending in the parallelepiped direction, the second-order primary vibration mode is bending in the transverse direction, and the third-order primary vibration mode is torsion. By comparing the first three orders of self-oscillation frequencies with the single tower model in Section III-A, it is found that the differences are significant, and the first three orders of self-oscillation frequencies in the tower-line system are smaller than those in the single tower by 9.67%, 8.31%, and 50.16%. We can see that the conductor and ground wire have a significant effect on the dynamic characteristics of the transmission tower, so the effect of the conductor and ground wire on the transmission tower needs to be considered in the study of the wind response of the tower-line system under downburst.

According to the different ways of wind load loading, the transmission tower and line calculation model is divided into a tower-line coupling system and a tower-line separation system. The tower-line coupling system is the transmission tower and transmission line through the insulator coupled into a system, at the same time on the transmission tower, insulators, conductors, and ground wires to apply the corresponding downburst wind load. The tower-line separation system first calculates the transmission conductor and ground wire, insulators subjected to wind loads, followed by the insulator, conductor, and ground wire according to the intrinsic properties of gravity calculated. The two kinds of loads are centralized loads, which are finally applied to the transmission tower and the insulator junction. This is equivalent to using the total wind load and gravity of the conductor and ground wire to the transmission tower.

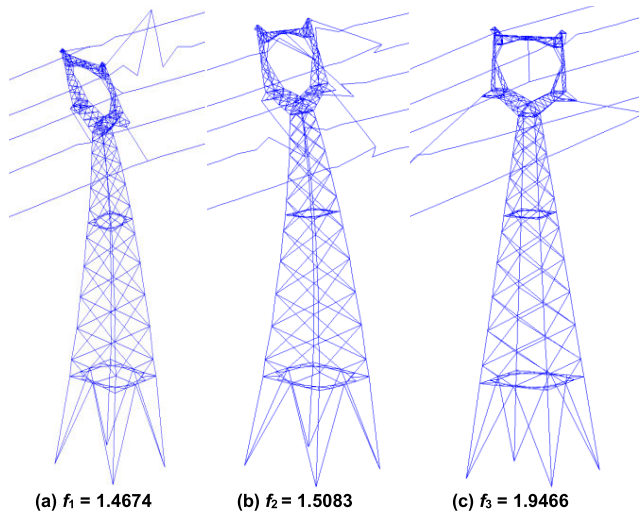


FIGURE 10. The first three main vibration modes of the transmission tower-line system.

IV. ANALYSIS OF WIND VIBRATION RESPONSE OF TRANSMISSION TOWER-LINE SYSTEM

A. MOST UNFAVORABLE WIND ANGLE OF ATTACK

The dynamic response of the transmission tower-line system under downburst is calculated by selecting 0°, 45°, 60°, and

90° wind angles of attack. The nodal displacement response of the transmission tower-line system in the X and Y directions is given in Figure 11. From Figure 11, it can be seen that in the X-direction, with the increase of the wind angle of attack, the conductor and ground wire increase the overall wind area and transfer the wind load to the tower through the insulators, which increases the displacement of each node in the X-direction. The peak displacement of the top of the tower reaches 1.28 m at the angle of attack of 90°. In the Y-direction, with the increase of the wind angle of attack, the overall wind area decreases, and the tension of the conductor and ground wire reduces the displacement response of the transmission tower, making the displacement response of the system gradually smaller. In a comprehensive analysis, 90° is the most unfavorable wind angle of attack, and subsequent calculations are used at a 90° wind angle of attack.

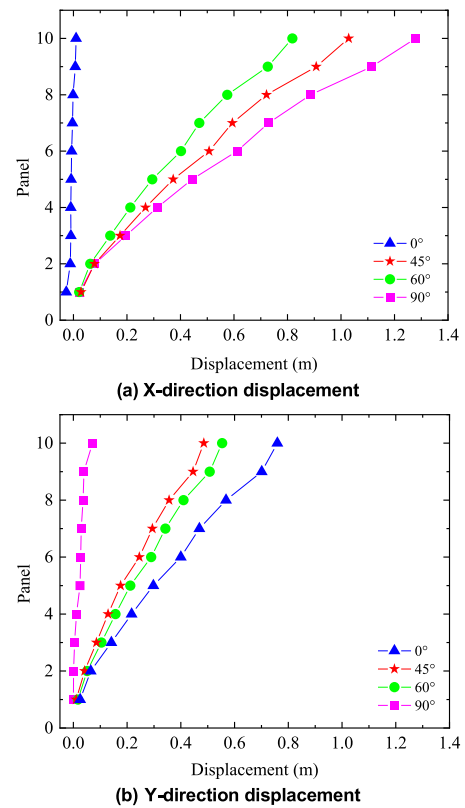


FIGURE 11. Displacement of transmission tower-line system under different wind angles of attack.

B. ANALYSIS OF WIND VIBRATION RESPONSE OF TWO SYSTEMS UNDER DOWNBURST

The displacement and acceleration time histories at the height nodes of the transmission tower are shown in Figure 12. Figure 12 shows that the displacement and acceleration responses of the tower-line separated system under the downburst are more significant than the corresponding responses of the coupled system. As the height increases, the response difference becomes more apparent. This is because the wind

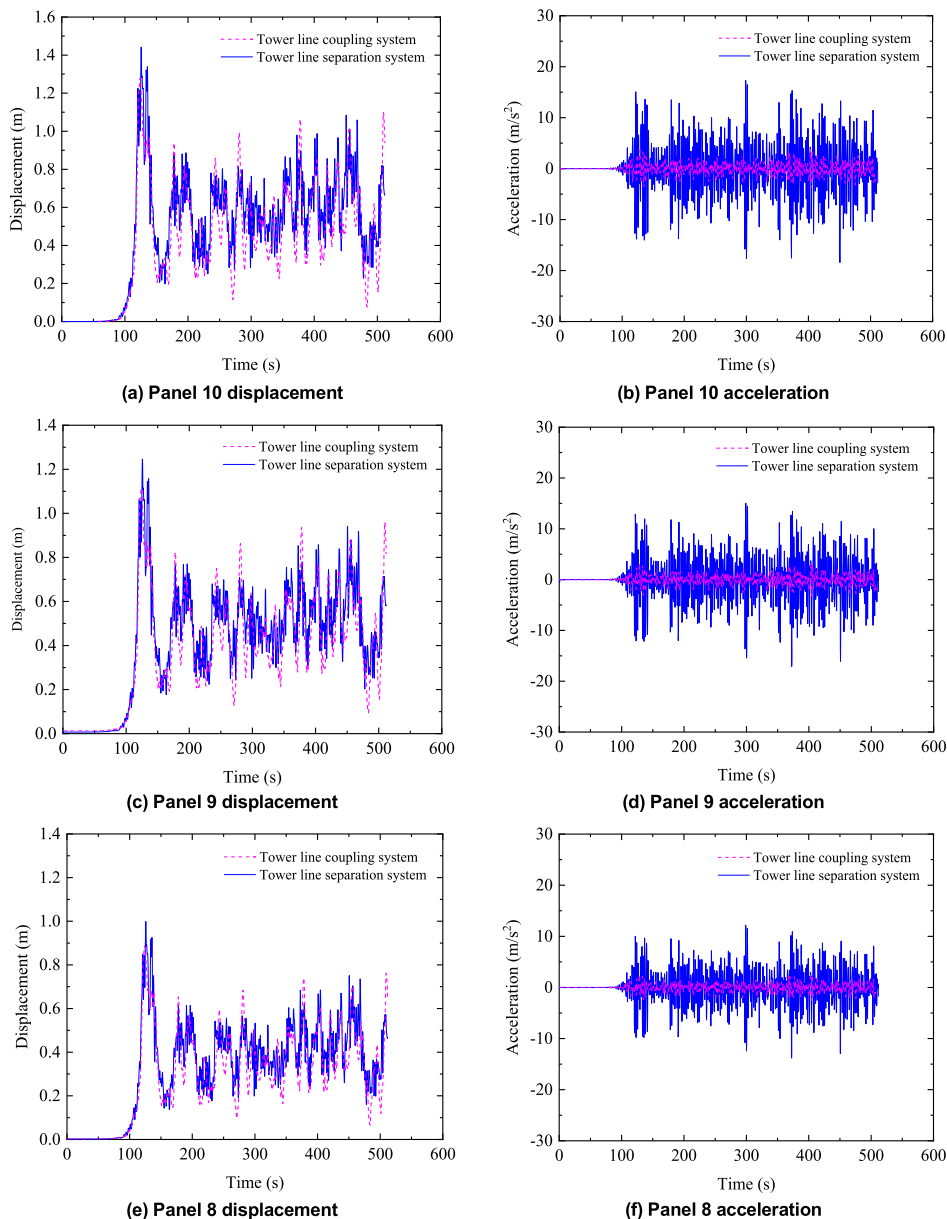


FIGURE 12. Time history of displacement and acceleration at the height node of the transmission tower.

speed will show an increasing trend before the downburst reaches the maximum peak height, and the height of the top of the tower is close to the height of the maximum wind speed of the downburst, so the displacement at the top of the tower reaches the peak.

The peak displacements and mean displacements at each node of the transmission tower under the downburst for both tower-line systems are given in Figure 13. From Figure 13, the peak displacement at each node for the tower-line separation system is more significant than that for the tower-line coupling system. The difference in peak displacement at the top of the tower is 12.68%. The displacement mean value of the tower-line separation system is greater than the tower-line

coupling system at all nodes. The difference in the displacement mean value at the top of the tower is 12.44%.

Figure 14 shows the peak acceleration and standard deviation of acceleration at each node for both tower-line systems under downburst. From Figure 14, we can see that the peak acceleration and standard deviation of acceleration for the tower-line separation system are more significant than the values for the tower-line coupling system. At the top of the tower, the peak acceleration and standard deviation of the tower-line separation system are 3.93 and 4.68 times higher than those of the tower-line coupling system. Under the downburst wind load, the insulators, conductors, and ground wires hanging under the transmission

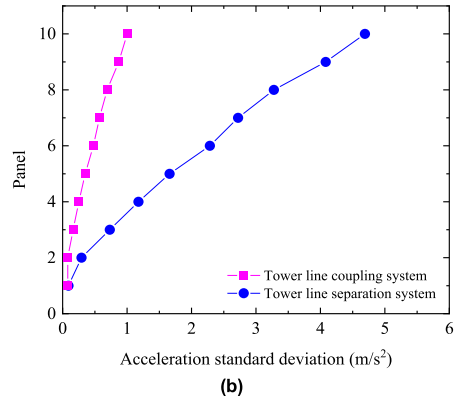
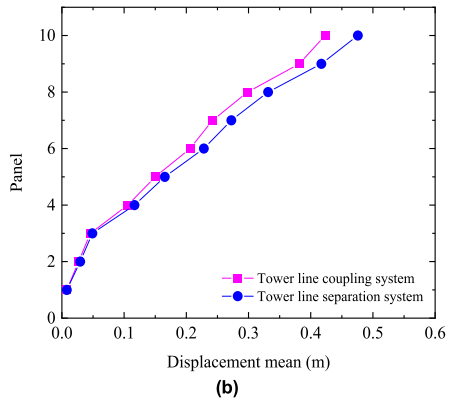
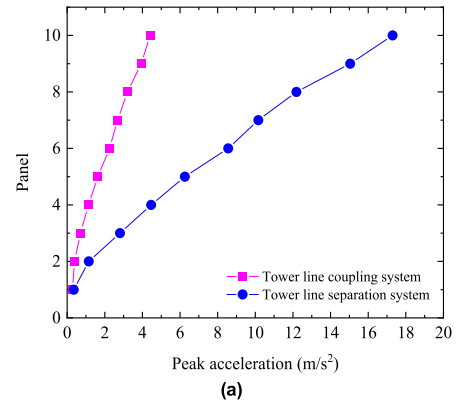
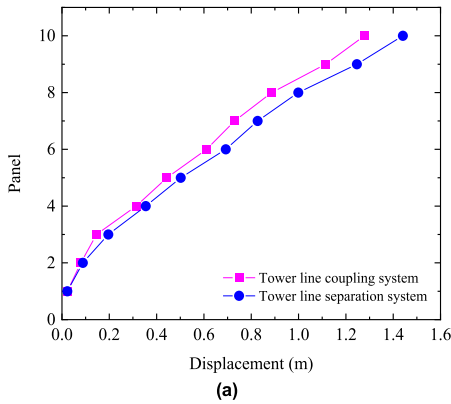


FIGURE 13. Displacement response and the mean value of displacement response at each height node of the transmission tower.

FIGURE 14. Peak acceleration response and acceleration standard deviation at each height node of the transmission tower.

tower cross-arms will swing back and forth, dissipating part of the energy of the transmission tower under wind load and reducing the displacement and acceleration response of the tower-line coupled system. However, in the tower-line separation system, the wind loads on insulators, conductors, and ground wires are always applied in the form of concentrated force on the nodes connecting insulators and transmission towers, which increases the displacement and acceleration response of the tower-line separation system.

The density curve of the acceleration power spectrum at the top of the transmission tower is given in Figure 15. From Figure 15, we can see that in the tower-line separation system, because there is only one primary vibration mode, only one excellent frequency appears in the tower-top acceleration power spectrum. In contrast, the signal energy generated by other minor modes is relatively tiny. In the tower-line coupling system, there are multiple vibration modes. The system is coupled with each other, and obviously, two excellent frequencies appear in the acceleration power spectrum. The results indicate that the tower-line coupling effect must be considered when performing transmission tower design.

C. DIFFERENT Z_{max}

The height Z_{max} at which the maximum wind speed of the downburst changes with the environment due to the influence of space-time and topography. Following the method

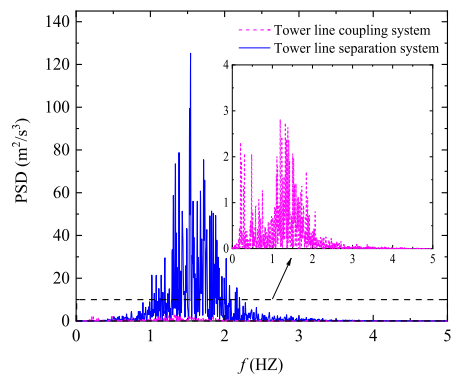


FIGURE 15. PSD of tower top acceleration for different tower-line systems.

described in Section II-C, the downburst wind speed time histories are obtained for heights of Z_{max} of 10 m, 30 m, 50 m, 70 m, 90 m, and 110 m, which are then analyzed in terms of power time histories for the two tower-line systems.

The peak displacement response of each height node of the two tower-line systems under downburst at different Z_{max} is given in Figure 16. From Figure 16, we can see that when Z_{max} is in the range of 10-70 m, the peak displacements of each height node of the transmission tower increase continuously with the rise of Z_{max} . At $Z_{max} = 70$ m, the transmission tower displacement response reaches its maximum value.

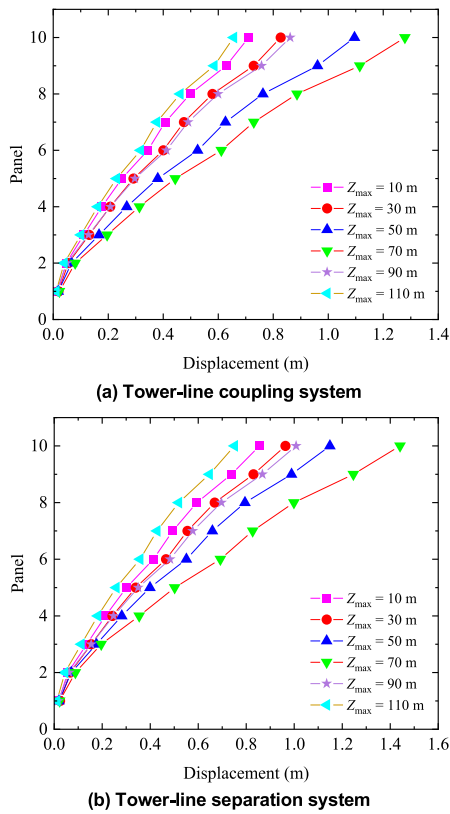


FIGURE 16. Displacement response of each node of two tower-line systems under different Z_{max} of downburst.

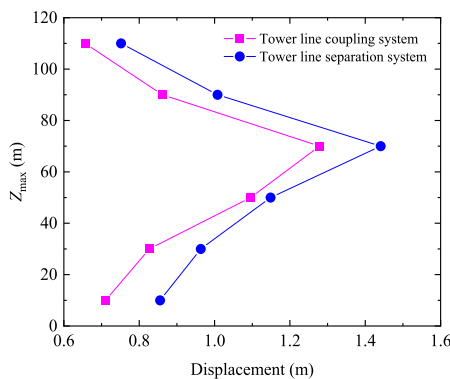


FIGURE 17. Maximum displacement of the vertex under downburst with different Z_{max} .

At this time, the peak wind speed of the downburst will act on the transmission tower, and its wind load contributes more to the displacement response of the tower than other conditions. When Z_{max} is 90-110 m, the height of the peak wind speed of the downburst exceeds the height of the transmission tower, and as Z_{max} continues to rise, the total wind load on the tower decreases with the increase of Z_{max} , and thus the peak displacement of the nodes at each height of the tower decreases.

Extracted vertex displacement maps of the two tower-line systems under the action of downburst flow at different Z_{max} are shown in Figure 17. Figure 17 shows that the maximum

vertex displacement of the tower-line separation system is always more significant than the corresponding displacement of the tower-line coupling system for $Z_{max} = 10-110$ m. The maximum vertex displacement of the tower-line separation system is 1.44 m for $Z_{max} = 70$ m and 1.44 m for the tower-line coupling system. At $Z_{max} = 70$ m, the vertex displacement of the tower-line separation system is 1.44 m, and the vertex displacement of the tower-line coupling system is 1.28 m. The relative displacement response difference reaches the maximum, and the maximum difference is about 11.1%, at which time the tower-line coupling effect is significant.

D. DIFFERENT TRANSMISSION LINE SPAN DISTANCE

In the actual project, the transmission tower-line system will be affected by the terrain or transmission line distance and other factors so it will have different spacing. Therefore, we selected four different spacings, such as 150 m, 250 m, 350 m, and 450 m, to analyze the tower-line system under different spacings. The time history of tower top displacements for the two tower-line systems is given in Figure 18.

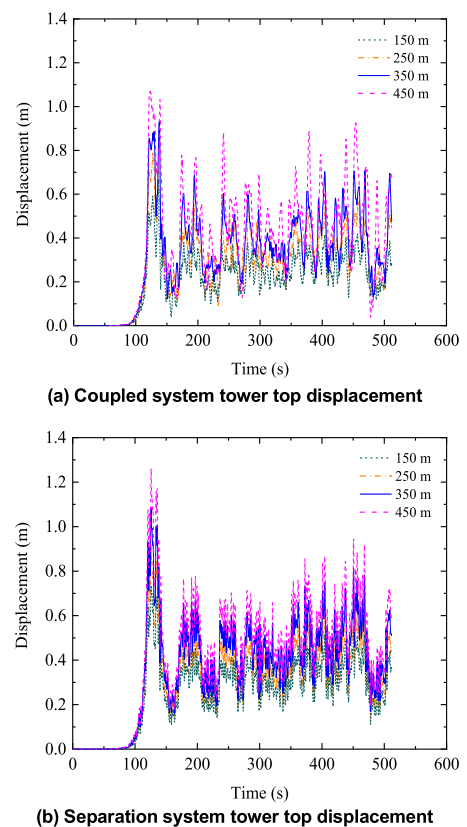
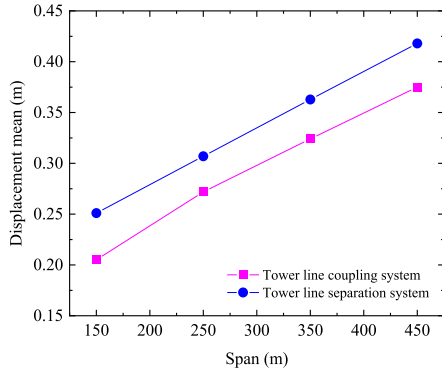


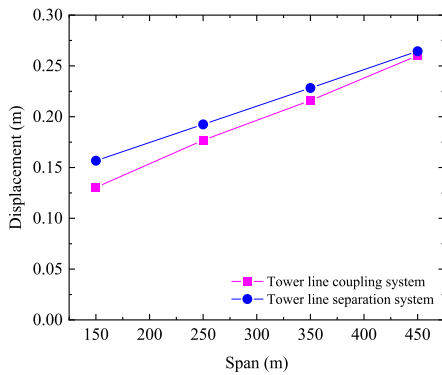
FIGURE 18. Time history of tower top displacements for two tower-line systems with different spacings.

Figure 19 compares tower top displacements of the two tower-line systems at different spacings. From Figure 19, it is shown that with the increase of spacing, the tower top displacement and the standard deviation of displacement become more extensive, which is because the windward area

of the conductor and ground wire increases with the increase of spacing, so the wind load on the conductor and ground line increases, increasing the tower top displacement and the standard deviation of displacement for the two tower-line systems.



(a) Mean value of tower top displacement

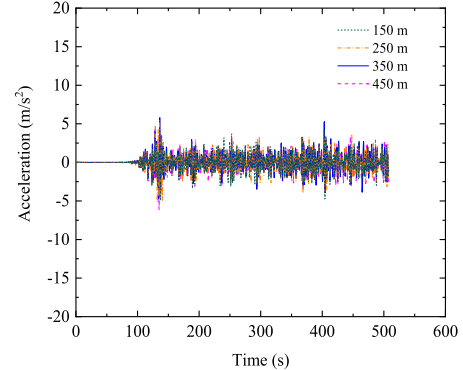


(b) Standard deviation of tower top displacement

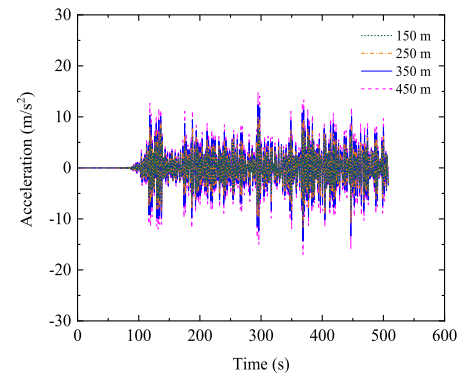
FIGURE 19. Mean and standard deviation of tower top displacements for two tower-line systems with different spacings.

Figure 20 gives the time history of tower top acceleration for the two tower-line systems at different spacings. Figure 20(a)-(b) shows that the tower top acceleration of the tower-line coupled system decreases with increasing spacing. In contrast, the opposite is true for the tower-line separated system. Figure 21 gives the standard deviation and difference of tower top acceleration for both tower-line systems at different spacings. From Figure 21(a), the standard deviation of the tower top acceleration for the tower-line separated system increases with increasing spacing. In contrast, the opposite is true for the tower-line coupled system. This is because the increase in spacing makes the transmission line longer, which makes the damping effect of the transmission line on the tower more prominent, resulting in a decrease in the standard deviation of acceleration for the tower-line coupled system. The tower-line separation system is not subject to the damping effect of the transmission line, and the length of the transmission line increases the area of the transmission tower subjected to wind load, resulting in the standard deviation of the acceleration of the tower-line separation system

rising with the increase of the spacing. From Figure 21(b), we can see that the difference in the standard deviation of the acceleration of the two tower-line systems increases with the spacing increase, and the tower-line coupling effect is significant.



(a) Coupled system tower top acceleration

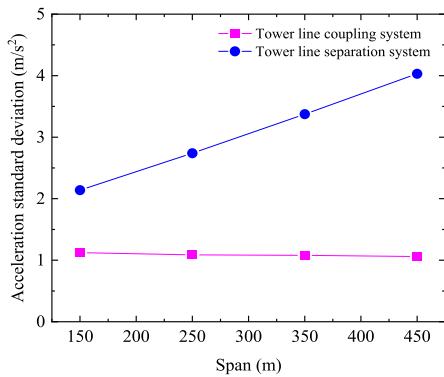


(b) Separation system tower top acceleration

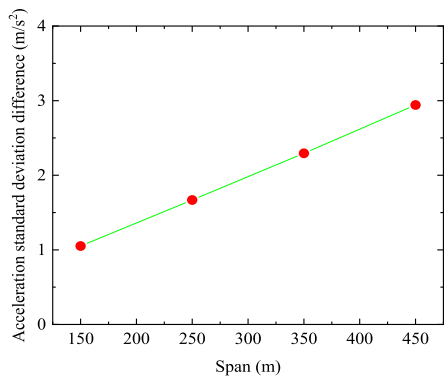
FIGURE 20. Time history of tower top acceleration for two tower-line systems with different spacings.

E. DESIGN REDUCTION COEFFICIENT FOR TOWER-LINE COUPLING EFFECTS

By analyzing the dynamic response of the tower-line coupling system and the tower-line separation system, the response of the tower-line separation system is larger than the corresponding response of the tower-line coupling system under various working conditions. In the traditional transmission tower load design specification, the transmission tower response is more significant than that of the transmission tower in the actual project, and this design result is conservative, which will cause steel waste and is not economical. The wind load must be corrected to comply with the actual project. Considering that the response trend of the tower-line coupling system and tower-line separation system under downburst flow is the same, meanwhile, the downburst wind is time-varying, the wind load reduction coefficient $A_z(z)$ of the tower-line separation system is defined as the ratio of the maximum value of the response of the tower-line coupling system to the maximum value of the response of the tower-line separation



(a) Standard deviation of tower top acceleration



(b) Standard deviation difference of tower top acceleration

FIGURE 21. Standard deviation and difference of tower top acceleration for two tower-line systems with different spacings.

system, which is expressed as follows:

$$A_z(z) = \frac{d_{tcs}}{d_{tss}} \quad (6)$$

where d_{tcs} is the maximum value of the response of the tower-line coupled system under the downburst, d_{tss} is the maximum value of the response of the tower-line separated system under the downburst.

By analyzing the influence of different Z_{max} and spacing on the tower-line coupling effect, it is obtained that the tower-line coupling effect is different under different parameters, and different $A_z(z)$ is calculated according to Eq. (6), and the calculation results are shown in Figure 22. From Figure 22, we can see that the value of $A_z(z)$ under the influence of different spacing ranges from 0.85 to 0.90, and under the influence of different Z_{max} , the value ranges from 0.83 to 0.95. In summary, it is suggested that the reduction coefficient of the coupling effect of the tower line under the downburst is more reasonable to take the value between 0.83-0.95.

To verify the reasonableness of the reduction coefficient of the tower-line coupling effect under the downburst proposed in this paper, a tower type different from the one above is selected for testing. The familiar T-type transmission tower in the actual project is selected for verification. The height of the tower is 86.9 m. The transmission tower components

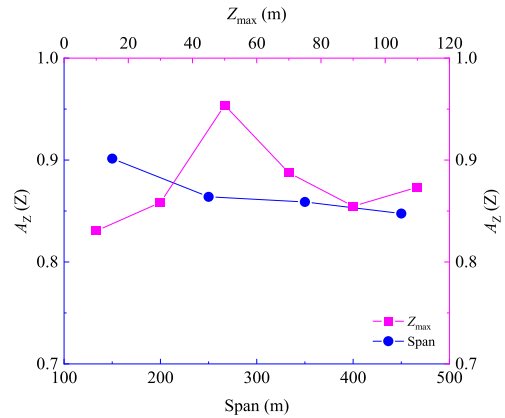


FIGURE 22. Effect of different Z_{max} and spacing on the reduction coefficient $A_z(z)$.

are BEAM188 elements, and the transmission conductors and ground wires are LINK10 elements, of which the main, diagonal, and auxiliary materials are the same as the steel types of the transmission tower in Section III-A. Constrain the four endpoints at the bottom of the transmission tower and the four endpoints of the transmission line. The transmission conductor and ground wire are 550 m long and divided into two layers, the upper two layers are ground wires, the lower two are conductors, and the conductor and ground wire are coupled with the transmission tower through insulators. The finite element model is shown in Figure 23.

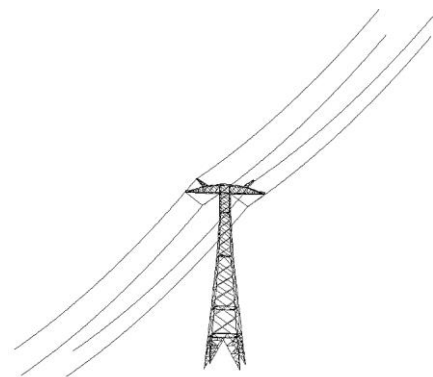


FIGURE 23. Finite element modeling of tower-line of T-type transmission tower.

The maximum displacement response of each node of the transmission tower is obtained by applying the downburst wind load to the tower-line coupling system and the tower-line separation system, as shown in Figure 24. From Figure 24(a), we can see that the maximum displacement response of the tower-line coupling system under the downburst is smaller than that of the tower-line separation system. The reduction coefficient $A_z(z)$ is calculated by Eq. (6) to be 0.88, which is within the recommended interval of this paper. The reduction coefficient calculates the wind load, and the response is analyzed in ANSYS. From Figure 24(b),

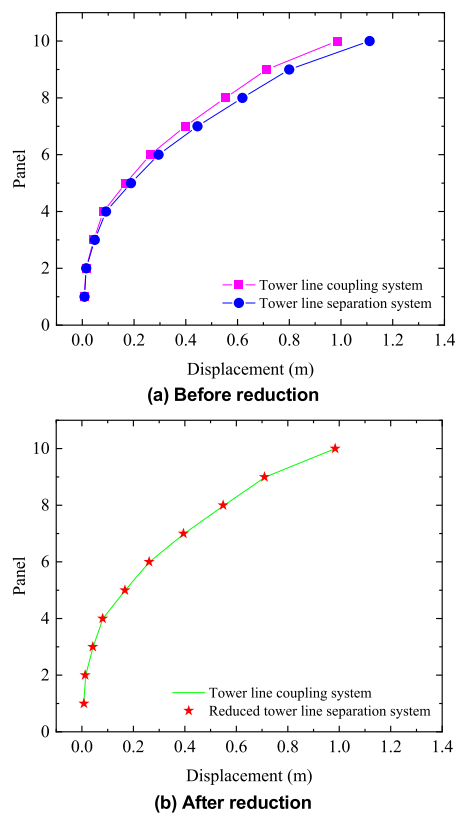


FIGURE 24. Comparison of the displacement response of the two systems before and after reduction.

we can see that the displacement responses of the two systems after reduction are in good agreement, which verifies the reasonableness of the reduction coefficient of the tower-line coupling effect under the downburst suggested in this paper.

V. CONCLUSION

In this paper, the downburst wind speed time histories are first generated by the superposition of the average wind speed and pulsating wind speed. Then, the finite element model of the transmission tower-line system is established. The wind vibration response of different tower-line systems is analyzed after determining the most unfavorable wind angle of attack of the downburst. Subsequently, the response and coupling effects of the tower-line system under different Z_{\max} and spacing parameters are investigated. Finally, the design reduction coefficient of the tower-line coupling effect is proposed on this basis. The following conclusions are obtained:

- 1) The dynamic time course analysis of the transmission tower and line system under different wind angles of attack determines that 90° is the most unfavorable wind angle of attack. Under the most unfavorable wind angle of attack, the mean and peak displacement response and the peak and standard deviation acceleration response of the tower-line separation system are more significant than those of the tower-line coupling system. With the increase in height, the difference in the responses of

the two systems is more significant. Compared with the tower-line separation system, the coupling system contains multiple vibration modes, and the coupling between the systems is apparent.

- 2) At $Z_{\max} = 10\text{--}110$ m, the maximum vertex displacement of the tower-line separation system is larger than the corresponding displacement of the tower-line coupling system. When $Z_{\max} = 70$ m, the difference between the top displacements of the two tower-line systems reaches the maximum value of about 11.1%, and the tower-line coupling effect is noticeable. With the increase of spacing, the tower top displacements and the standard deviation of the displacements under the two tower-line systems increase. In the tower-line separation system, the tower top acceleration increases with increasing spacing, while the opposite is true for the tower-line coupling system. In addition, the difference in the standard deviation of acceleration increases with increasing spacing for both tower-line systems, and the tower-line coupling effect is noticeable.
- 3) Based on the wind vibration response analysis results under different Z_{\max} and span distances, the design reduction coefficient for the coupling effect of transmission towers under downburst is further proposed. At the same time, it is suggested that the range of values between 0.83–0.95 is more reasonable. Finally, by choosing a different tower type for testing, the reasonableness of the proposed wind load reduction coefficient for the tower-line separation system is verified, and it can accurately consider the tower-line coupling effect. It has a specific reference value for further optimizing the transmission tower design.

REFERENCES

- [1] F. H. Proctor, "Numerical simulations of an isolated microburst. Part I: Dynamics and structure," *J. Atmos. Sci.*, vol. 45, no. 21, pp. 3137–3160, Nov. 1988.
- [2] R. P. Selvam and J. D. Holmes, "Numerical simulation of thunderstorm downdrafts," *J. Wind Eng. Ind. Aerod.*, vol. 44, no. 1, pp. 2817–2825, Oct. 1992.
- [3] M. R. Hjelmfelt, "Structure and life cycle of microburst outflows observed in Colorado," *J. Appl. Meteorol.*, vol. 27, no. 8, pp. 900–927, Aug. 1988.
- [4] P. McCarthy and M. Melsness, "Severe weather elements associated with September 5, 1996 hydro tower failures near Grosse Isle, Manitoba, Canada," Manitoba Environ. Service Centre, Environ. Canada, Winnipeg, MB, Canada, 1996, p. 21.
- [5] G. S. Wood, K. C. S. Kwok, N. A. Motteram, and D. F. Fletcher, "Physical and numerical modelling of thunderstorm downbursts," *J. Wind Eng. Ind. Aerodynamics*, vol. 89, no. 6, pp. 535–552, May 2001.
- [6] C. W. Letchford and M. T. Chay, "Pressure distributions on a cube in a simulated thunderstorm downburst. Part B: Moving downburst observations," *J. Wind Eng. Ind. Aerodynamics*, vol. 90, no. 7, pp. 733–753, Jul. 2002.
- [7] A. Sengupta, F. L. Haan, P. P. Sarkar, and V. Balaramudu, "Transient loads on buildings in microburst and Tornado winds," *J. Wind Eng. Ind. Aerodynamics*, vol. 96, nos. 10–11, pp. 2173–2187, Oct. 2008.
- [8] E.-S. Abd-Elaal, J. E. Mills, and X. Ma, "Numerical simulation of downburst wind flow over real topography," *J. Wind Eng. Ind. Aerodynamics*, vol. 172, pp. 85–95, Jan. 2018.
- [9] Z. Fang, Z. Wang, Z. Li, J. Yan, and H. Huang, "Wind field characteristics of stationary and moving downbursts based on the test of impinging jet with a movable nozzle," *J. Wind Eng. Ind. Aerodynamics*, vol. 232, Jan. 2023, Art. no. 105266.

- [10] A. Y. Shehata, A. A. El Damatty, and E. Savory, "Finite element modeling of transmission line under downburst wind loading," *Finite Elements Anal. Des.*, vol. 42, no. 1, pp. 71–89, Oct. 2005.
- [11] X. Fu, H.-N. Li, and G. Li, "Fragility analysis and estimation of collapse status for transmission tower subjected to wind and rain loads," *Struct. Saf.*, vol. 58, pp. 1–10, Jan. 2016.
- [12] A. El Damatty and A. Elawady, "Critical load cases for lattice transmission line structures subjected to downbursts: Economic implications for design of transmission lines," *Eng. Struct.*, vol. 159, pp. 213–226, Mar. 2018.
- [13] Y. Zhao, Q. Sun, Z. Song, D. Wang, and X. Wang, "A dynamic responses and evaluation method of the downburst wind loads effect on a transmission tower," *J. Vib. Shock*, vol. 40, no. 12, pp. 179–188, Jun. 2021.
- [14] M. Liu, L. Huang, and Z. Xie, "Wind tunnel testing of aeroelastic transmission tower under thunderstorm wind and boundary layer wind," *High Voltage Eng.*, vol. 48, no. 2, pp. 594–602, Apr. 2022.
- [15] D. Yu and G. Li, "A novel woodbury solution method for nonlinear seismic response analysis of large-scale structures," *Earthq. Eng. Struct. Dyn.*, vol. 53, no. 1, pp. 261–278, Jan. 2024.
- [16] X. Fu, Z.-X. Tan, H.-N. Li, and G. Li, "Static and dynamic response characteristics of a full-scale long-cantilever tower under various loading conditions," *J. Struct. Eng.*, vol. 149, no. 5, May 2023, Art. no. 05023002.
- [17] K. J. Alawode, Z. Azzi, A. Elawady, and A. G. Chowdhury, "Dynamic properties of an aeroelastic transmission tower subjected to synoptic and downburst-like outflows," *J. Wind Eng. Ind. Aerodynamics*, vol. 242, Nov. 2023, Art. no. 105557.
- [18] Y. Guo, "Studies on wind-induced dynamic response and vibration control of long span transmission line system," Ph.D. dissertation, Coll. Civil Eng. Arch., Zhejiang Univ., Hangzhou, China, 2006.
- [19] B. He, M. Zhao, W. Feng, Y. Xiu, Y. Wang, L. Feng, Y. Qin, and C. Wang, "A method for analyzing stability of tower-line system under strong winds," *Adv. Eng. Softw.*, vol. 127, pp. 1–7, Jan. 2019.
- [20] T. Li, "Static stress calculation and analysis of high voltage transmission line tower-line coupling under strong wind," *Electr. Power Sci. Eng.*, vol. 36, no. 12, pp. 68–73, Dec. 2020.
- [21] W. Zhang, Y. Xiao, and C. Li, "Strong wind-induced vibration analyses of uncoupled transmission tower-line model," in *Proc. 5th Asia Conf. Power Electr. Eng. (ACPEE)*, Chengdu, China, Jun. 2020, pp. 1898–1902.
- [22] C. Wu, B. Zhang, Z. Liu, X. Yang, C. Li, and Y. Zhao, "Influence of different loading modes for wind-induced response of transmission towers," *Sci. Tech. Eng.*, vol. 22, no. 21, pp. 9238–9244, Jul. 28, 2022.
- [23] Y. Zhu, Y. Li, and Q. Xie, "Influence analysis of aerodynamic damping on transmission line System's wind-induced vibration," in *Proc. IEEE 6th Conf. Energy Internet Energy Syst. Integr. (EI2)*, Chengdu, China, Nov. 2022, pp. 1512–1517.
- [24] H. Zhang, "Study on coupling and destruction of transmission tower-line system in micro terrain," M.S. thesis, Coll. Civil Eng., Anhui Jianzhu Univ., Hefei, Anhui, China, 2022.
- [25] Z. Fang, Z. Wang, R. Zhu, and H. Huang, "Study on wind-induced response of transmission tower-line system under downburst wind," *Buildings*, vol. 12, no. 7, p. 891, Jun. 2022.
- [26] H. Hangan, D. Roberts, Z. Xu, and J. Kim, "Downburst simulation. Experimental and numerical challenges," in *Proc. 11th Int. Conf. Wind Eng.*, Lubbock, TX, USA, 2003, pp. 2241–2248.
- [27] M. Mason, C. W. Letchford, and G. Wood, "Physical simulation of thunderstorm downbursts for wind engineering applications," in *Proc. Int. Conf. Storms*, Melbourne, VIC, Australia, 2004, pp. 236–237.
- [28] W. Qu, B. Ji, J. Li, and J. Wang, "The study on numerical simulation of downburst wind," *J. Earthq. Eng. Eng. Vib.*, vol. 28, no. 5, pp. 133–139, Oct. 2008.
- [29] D. D. Vicroy, "Assessment of microburst models for downdraft estimation," *J. Aircr.*, vol. 29, no. 6, pp. 1043–1048, Nov. 1992.
- [30] R. M. Oseguera and R. L. Bowles, *A Simple, Analytic 3-Dimensional Downburst Model Based on Boundary Layer Stagnation Flow*. Hampton, VA: Langley Research Center, Jul. 1988.
- [31] Y. Yao, L. Su, M. Li, Y. Chu, and H. Huang, "Wind load characteristics of double-sided spherical shell roof under downburst," *J. Jilin Univ. Eng. Tech.*, vol. 52, no. 3, pp. 615–625, Dec. 2022.
- [32] L. Chen and C. W. Letchford, "A deterministic–stochastic hybrid model of downbursts and its impact on a cantilevered structure," *Eng. Struct.*, vol. 26, no. 5, pp. 619–629, Apr. 2004.
- [33] M. T. Chay, "Physical modelling of thunderstorm downbursts for wind engineering applications," M.S. thesis, Dept. Civil Environ. Eng., Texas Tech Univ., Austin, TX, USA, 2001.
- [34] Y. Jiang, N. Zhao, L. Peng, J. Xin, and S. Liu, "Fast simulation of fully non-stationary wind fields using a new matrix factorization assisted interpolation method," *Mech. Syst. Signal Process.*, vol. 172, Jun. 2022, Art. no. 108973.
- [35] E. Savory, G. A. R. Parke, M. Zeinoddini, N. Toy, and P. Disney, "Modelling of Tornado and microburst-induced wind loading and failure of a lattice transmission tower," *Eng. Struct.*, vol. 23, no. 4, pp. 365–375, Apr. 2001.
- [36] B. Zhu, "Research on wind-induced response of UHV guyed single-mast transmission tower-line system," M.S. thesis, Coll. Energy Power Mech. Eng., North China Electr. Power Univ., Beijing, China, 2016.
- [37] S. Meng and L. Shan, "Form-finding in dynamics analysis of transmission line," *Power Syst. Clean Energy*, vol. 25, no. 10, pp. 43–47, Oct. 2009.



YONGLI ZHONG was born in China. He received the B.S. degree from Huazhong University of Science and Technology and the Ph.D. degree in civil engineering from Chongqing University. His research interests include the response of the transmission line under the downburst and the ice shedding of the conductor.

YICHEN LIU was born in China. He received the B.S. degree from Chongqing University of Science and Technology, Chongqing, China, in 2022, where he is currently pursuing the M.S. degree. His research interest includes the response of transmission lines under downburst.

SHUN LI was born in China. He received the B.S. and M.S. degrees from Chongqing University of Science and Technology, in 2020 and 2023, respectively. His research interest includes the response of transmission lines under downburst.



ZHITAO YAN was born in China. He received the M.S. and Ph.D. degrees from Chongqing University. He is currently a Professor. His research interests include the galloping of transmission lines and the dynamics of structures.



XINPENG LIU was born in China. He received the Ph.D. degree from Chongqing University, in 2016. His research interests include structural wind engineering, structural intelligent computation, and system parameter inversion.

...